High-order harmonic generation in a microfluidic glass device

Journal of Physics: Photonics

OPEN ACCESS

RECEIVED
12 December 2019

REVISED
7 February 2020

ACCEPTED FOR PUBLICATION
6 March 2020

PUBLISHED
9 April 2020

PAPER

High-order harmonic generation in a microfluidic glass device

A G Ciriolo[1,6], R Martínez Vázquez[1,6], V Tosa[2], A Frezzotti[3], G Crippa[4], M Devetta[1], D Facciálá[1], F Frassetto[5], L Poletto[5], A Pusala[1], C Vozzi[1], R Osellame[1] and S Stagira[1,4]

[1] Institute for Photonics and Nanotechnologies, National Research Council, Milano, Italy
[2] National Institute for R&D of Isotopic and Molecular Technologies, Cluj-Napoca, Romania
[3] Politecnico di Milano, Department of Aerospace Science and Technology, Milano, Italy
[4] Politecnico di Milano, Physics Department, Milano, Italy
[5] Institute for Photonics and Nanotechnologies, National Research Council, Padova, Italy

E-mail: annagabriella.ciriolo@polimi.it **and** caterina.vozzi@cnr.it

Keywords: high-order harmonics, attosecond science, femtosecond laser micromachining

Abstract

We report on the efficient generation of high-order harmonics in helium gas inside complex glass micro-devices fabricated by femtosecond laser micromachining. By exploiting the three-dimensional capabilities and extreme flexibility of this fabrication technique we developed fluidic micro-structures in a fused-silica substrate that allowed us to achieve accurate control of the gas density inside a micrometer-sized microchannel. As a result, we achieved a broadband spectrum of extreme ultraviolet (XUV) radiation which extends up to 200 eV and we observed a considerable increase in the harmonics generation efficiency if compared with traditional harmonic generation in gas jets. We foresee that the application of femosecond-laser-micromachined glass devices to high-order harmonics generation can be extended to more complex on-chip systems including different functionalities, thus opening the possibility to future miniaturization of XUV and Attosecond beamlines.

1. Introduction

High-order Harmonic Generation (HHG) is a strongly non-linear optical process driven by intense and ultrashort laser pulses in matter. This process involves the emission of a burst of coherent radiation, collinear to the driving beam, with a characteristic comb-like spectrum of odd harmonics of the fundamental laser field, ranging from the vacuum ultraviolet to the soft x rays [1–3].

Since its first observation more than twenty years ago [4, 5], HHG has been considered as a promising source for extreme ultraviolet (XUV) spectroscopy. Furthermore, due to the temporal structure of the XUV emission, HHG is routinely exploited for Attosecond Pulse Generation (APG). HHG and APG currently provide a cutting-edge technology for studying ultrafast dynamics in atoms, molecules and condensed matter with temporal resolutions on the attosecond time-scale [6].

Up to now, despite the potentials for numerous applications in the field of ultrafast spectroscopy and high-resolution imaging, coherent light sources of XUV and soft x-rays based on HHG are confined to a few advanced laboratories and large-scale facilities [7], due to their high technological complexity. In this work, we demonstrate for the first time the generation of high order harmonics in noble gas in a glass microfluidic device fabricated through femtosecond laser micromachining. This result opens the extremely attractive perspective of developing more compact and easy-to-handle XUV and attosecond beamlines.

Currently, the advances in micromachining techniques are boosting a great impulse towards the miniaturization of optical systems. In particular, Femtosecond Laser Micromachining (FLM) is playing a leading role in the field of integrated photonics and microfluidics [8–10]. This technique allows to fabricate microstructures in transparent materials by focusing ultrashort laser pulses. In the focal region, non-linear optical processes, like multiphoton and avalanche ionization, occur, which produce a permanent modification of the structural and chemical properties of the target material. Under suitable exposure

[6] These authors contributed equally to this work.

conditions, the material undergoes a laser-induced nanostructuring, the so-called 'nanogratings', that result in a preferential chemical etching of the irradiated regions [11]. By moving the laser focus inside the substrate it is possible to draw arbitrary three-dimensional modifications that can be selectively removed in a subsequent chemical etching step. Femtosecond Laser Irradiation followed by Chemical Etching (FLICE) allows the realization of complex hollow microstructures in glass. Due to its unique performances in terms of flexibility and 3D capabilities, FLICE has been successfully exploited for the fabrication of lab-on-chip devices [12, 13]. In this framework, FLICE devices have been mainly thought for applications related to the transport of liquids, but they can also be used for shaping and controlling gas fluxes [14]. We will show that such hollow architectures can be extended to applications involving intense optical beams.

In this framework, gas-filled Hollow-Core Fibers (HCF) and Photonic-Crystal Fibers (PCF) are widely exploited in the field of ultrafast laser sources for the compression of intense pulses [15, 16], for the generation of ultrashort pulses in a wide range of spectral regions by parametric frequency conversion [17–20] and for the generation of high-order harmonics spectra up to 1-keV photon energy by mid-IR driving pulses [21]. However, if compared to traditional HCFs and PCFs, FLICE microstructures provide the advantage that different functionalities can be integrated within the same device, including microfluidics, pulse shaping along micro-structured capillaries, optical filtering and spectral dispersion by micro-gratings.

The micromachined device used in this work is composed of a network of gas delivery microchannels and of a main cylindrical microchannel that acts as a hollow waveguide. By guiding ultrashort Ti:Sapphire laser pulses inside the gas-filled waveguide we observed efficient generation of high-order harmonics up to 200 eV. We explored the dependence of the HHG process on the local density of the interacting medium by complementing experimental measurements with gas dynamics modelling. We also performed numerical simulations of HHG taking into account the driving field confinement and showing the spectrum generated by the laser-gas interaction along the microchannel.

We believe that this scheme is extremely promising for applications in the field of HHG-based sources technology. We are working on extending this approach to more complex architectures, with the aim of realizing on-chip platforms for XUV and attosecond spectroscopy.

2. Materials and Methods

The design of the FLICE device is reported in figure 1(a). This device was realized inside a $10 \times 8 \times 1$ mm^3 fused silica plate. It consists of a $2 \times 4.7 \times 0.1$ mm^3 rectangular-like reservoir that is used as a chamber for distributing the gas inside an embedded microchannel which acts as a hollow waveguide for ultrashort laser pulses. The microchannel extends along the 8-mm glass length and has a diameter of 130 μm. It is connected to the reservoir through four equally-spaced microchannels, whose relative distance is 1.2 mm. These small channels have variable diameter from ~50 μm (at the reservoir base) to ~40 μm (at the hollow waveguide surface).

The fabrication of the glass microchip begins with the irradiation of the fused silica slab with a focused femtosecond laser beam. We used the second harmonic (515 nm) of a fiber laser (Satsuma, Amplitude) that is focused by a 63X (0.65 NA) microscope objective (LD-plan Neofluar, Zeiss). The laser repetition rate is set at 1 MHz, with a pulse duration of 230 fs and pulse energy of 300 nJ. The glass sample is mounted onto a high-resolution 3D movement system (Aerotech, ANT) and moved with respect to the laser beam following the desired trajectory. After the laser irradiation, the sample is immersed in an ultrasonic bath of a 20% HF aqueous solution at 35 °C for about 2 h.

A fundamental characteristic of FLICE technique is the possibility to realize structures with millimeter size (gas reservoir) and small structures with micrometer size (microchannels) in the same device with just one fabrication process, provided that a proper irradiation pattern is chosen. For this device, the irradiated pattern has been studied to compensate for inhomogeneous exposition to acid during the etching process to achieve a central channel with a constant radius after the etching step.

This device has been designed to work under vacuum and it is directly connected to a gas reservoir to obtain a continuous gas flow. To model the gas dynamics in the microchip we exploited Comsol Multiphysics [24]. In particular, we studied the gas flow through the device in the final steady-state. We applied the High Mach Number Flow model coupled with the so-called k-ε turbulence model in order to properly describe deviations from the laminar flow of the gas inside the device due to boundary effects. For the discretization of the geometry, we used a triangular mesh with cell dimensions varying between a maximum value of 70 μm and a minimum value of 7 μm depending on the size of the element composing the numerical domain (see the insert in figure 1(b)). The pattern of points of the mesh is automatically optimized by the software according to the physics of the problem.

The results are reported in figures 1(b) and (c) that show respectively the velocity map in the hollow microstructure and the gas density distribution along the channel axis. In steady conditions, the velocity

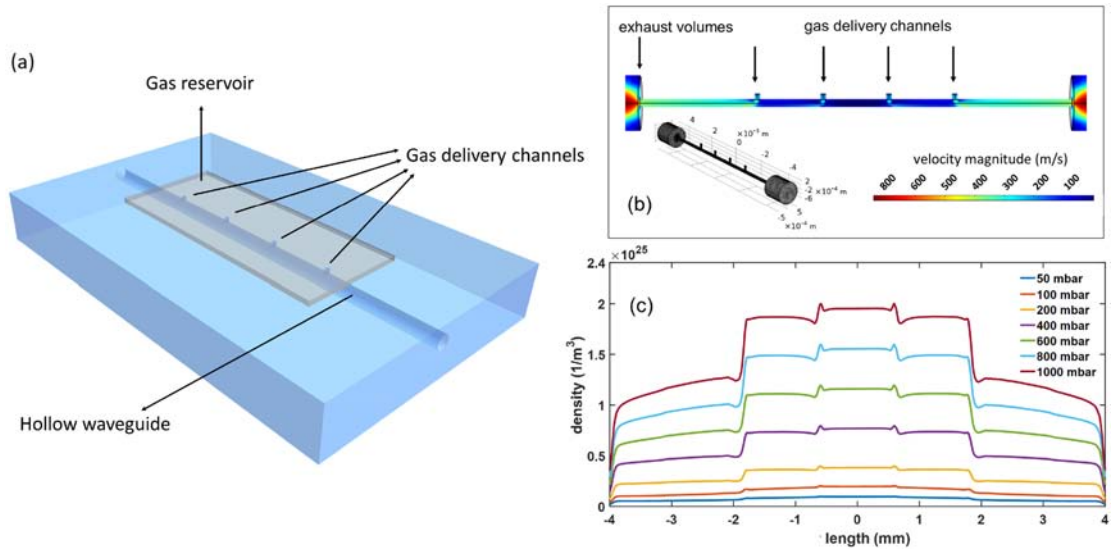

Figure 1. (a) Design of the micro-chip. On the right, numerical simulation of helium-gas fliudics inside the micromachined device, showing (b) the gas velocity and (c) the gas density along the central axis as a function of the backing pressure. The velocity map reported in panel (b) refers to a backing pressure of 1 bar. The insert in panel (b) shows the geometry and mesh of the simulated gas volume. The hollow waveguide and the small upper channels reproduce the chip internal structure. The two cylindrical structures placed at the extremities of the device are used as output volume for simulating the gas expansion in the interaction chamber. The simulations were performed using COMSOL Multiphysics.

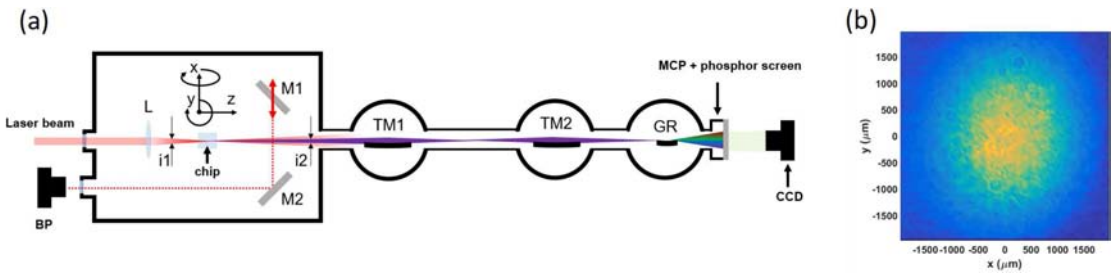

Figure 2. (a) High-order harmonics generation and acquisition setup. L, lens; M1, M2 mirrors; BP beam profiler; TM1, TM2 toroidal mirrors; GR grating; i1, i2 irises. (b) Hollow waveguide mode in the far field.

magnitude exhibits a uniform profile in the central part of the channel which is directly filled by the small injection channels (the backing pressure of the reservoir was set at 1 bar). Instead, an abrupt change in the behavior occurs in correspondence of the exits towards the vacuum chamber, where the gas undergoes a remarkable acceleration.

The gas density along the microchannel axis as a function of the pressure in the reservoir is reported in figure 1(c). The density profile depends on the structure of the gas injection module. In this device, due to the evenly distributed injection microchannels, an almost uniform gas density was achieved in the central part of the hollow waveguide which extends over a 3.6 mm length. Approaching the exits, the density undergoes a gradual decrease.

The gas density inside the channel scales linearly with the pressure in the reservoir. Thus, by monitoring the backing pressure, it was possible to achieve accurate control of the gas density in the hollow waveguide. This is of fundamental importance for such applications as HHG and APG that are strongly affected by collective effects due to the density and the spatial distribution of the generating medium. Indeed, the control of the generating medium is crucial for phase-matching purposes. This design offers a high flexibility upon changes of the number, shape and position of the micro-injectors, that can be arranged in a different way to give a suitable density profile.

3. Experimental Setup

A scheme of the experimental setup is reported in figure 2(a). A fraction of a Ti:Sapphire laser output (25 fs, 400–500 μJ, 1 kHz) was used for driving HHG inside the gas-filled FLICE device.

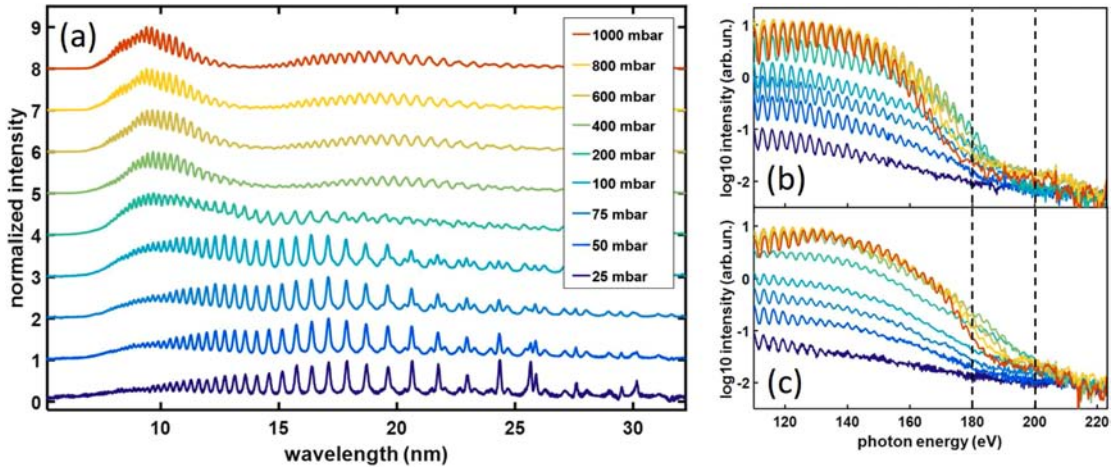

Figure 3. High-order harmonics spectra generated in helium at different backing pressures (from 25 to 1000 mbar) and at different driving pulse energy (420 μJ and 500 μJ). (a) HHG spectra generated by 500 μJ laser pulses and normalized to the intensity peak. (b)–(c) Log-scale HHG spectra (not normalized) at the cutoff plotted to the photon energy. The pulse energy is respectively 420 μJ and 500 μJ. Dashed lines are used in the high-energy region for the sake of comparison. The color mapping is the same for the three figures.

The beam was coupled in the microchannel by a lens. A focal length of 25 cm is chosen to achieve a high coupling efficiency (> 60%). To allow for a proper beam-to-waveguide positioning, we mounted the device on top of high-precision alignment stages.

The waveguide mode was monitored by a dedicated line with a mirror, mounted on a motorized linear stage, which could be inserted in the beam path, sending the beam to a beam profiler. The profile of the mode in the far field is shown in figure 2(b).

The gas was provided to the device through a pipe line that was directly interfaced with the mechanical mounting where the chip was placed. The gas density could be manually tuned by a needle valve mounted in the gas line, and the gas baking pressure was accurately monitored by a capacitive pressure gauge placed after such valve. The working pressure in the vacuum chamber where the HHG device was located ranged between 10^{-4} and 10^{-5} mbar depending on the gas backing pressure. The grazing incidence XUV spectrometer used for collecting the HHG radiation works in stigmatic configuration, with a toroidal mirror that focuses the HHG beam on a dispersion grating. The dispersed HHG signal is detected by a Micro-Channel Plate (MCP) followed by a phosphor screen. The image displayed on the phosphor screen is acquired by a CCD camera.

4. Results

Figure 3(a) shows different harmonics spectra generated inside the device filled with helium at different backing pressures. The energy of the ultrashort pulses used for driving HHG was 500 μJ. The pressure range explored goes from few tens of mbar up to 1 bar. Each spectrum is normalized to the peak and vertically shifted for the sake of clearness.

By changing the pressure, the HHG spectrum exhibits a reshaping. In particular, upon pressure increasing, the yield of the spectrum at shorter wavelengths undergoes an enhancement if compared to long wavelengths.

All the HHG spectra are affected by the second-order dispersion of the grating, which is responsible for the presence of extra-peaks at longer wavelengths. In particular, for high pressures (400–1000 mbar), the spectral features centered at 20 nm wavelengths are mostly artifacts due to a second-order-induced replica of the harmonics spectrum at 10 nm wavelengths.

In figures 3(b) and (c) we show the normalized HHG spectra at a driving pulse energy of respectively 420 μJ and 500 μJ (the latter one being the same energy as in figure 3(a)). In both cases, the pressure dependence of the cutoff is non-linear and a maximum extension of HHG can be observed for intermediate pressures. Concerning the generation yield, a considerable improvement can be observed by increasing the backing pressure up to 400 mbar, above which saturation occurs.

For helium, the energy of the driving pulses does not significantly affect the shape of the HHG spectrum. However, by increasing the pulse energy, the XUV spectrum becomes wider, extending up to 200 eV. The pressure dependence shown by the HHG yield is due to the combined effect of phase-matching and absorption from the gas. As the pressure increases, the XUV radiation is strongly absorbed in the 8-mm-long

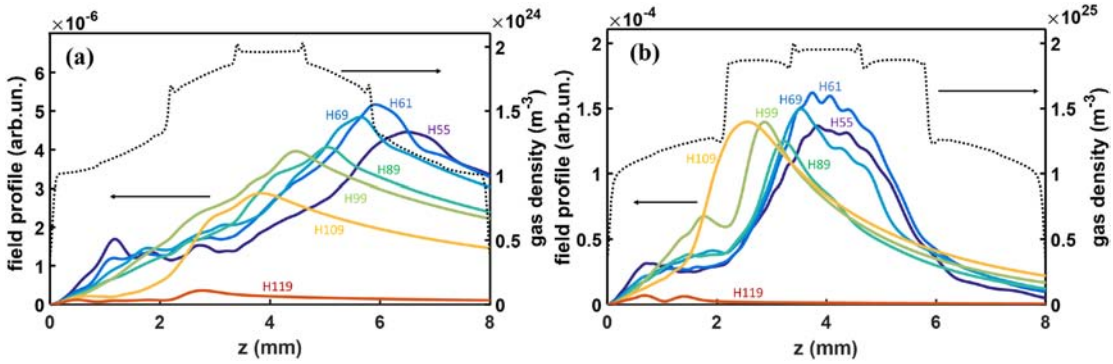

Figure 4. Field amplitude along the propagation axis (z) of a selected number of harmonics calculated for two different gas density distribution. The dotted line provides the gas density profile (m^{-3}) used in the two cases. The pressure in the reservoir used for obtaining the gas density profiles is (a) 100 mbar and (b) 1 bar.

waveguide, with an attenuation rate that is higher at longer XUV wavelengths. Moreover, the phase mismatch between the fundamental and the harmonic fields worsens leading to both a dramatic reduction of the yield mainly in the lower-energy part of the spectrum and a decrease of the cutoff extension.

For studying the harmonic generation process in the gas-filled hollow waveguide and its dependence on the gas density, numerical calculations were performed, accounting for collective effects of phase-matching and absorption on the XUV radiation and propagation effects on the driving laser field.

The numerical simulations have been carried out using a version of the 3D non-adiabatic model presented in [25], and adapted for laser pulse propagation in the waveguide. In the basic version we first solve the pulse propagation in the ionized gas medium and then calculate the atomic dipole induced by the propagated field using the strong-field approximation (SFA) [1]. The macroscopic harmonic signal is the result of the coherent superposition of the single dipole emissions in each spatial point. Since the model has been described in several papers [25–27], we only mention here some specific aspects connected to the driving pulse propagation in the waveguide.

The wave equation for pulse propagation is solved using the split operator method [28] in which one advances the solution from z to $z + dz$ in two steps, a first linear (diffraction) part corresponding to the homogeneous wave equation, and a second nonlinear one in which dispersion, ionization, and Kerr contributions are included. In the first step we write the electric field in frequency domain as a superposition of the hybrid EH_{1m} eigenmodes and advance the solution in the moving frame by calculating the new coefficients in $z + dz$ using the the coefficients in z and the propagation constants for the EH_{1m} eigenmodes in the circular hollow core fiber. The nonlinearity contribution is estimated in time domain while advancing the solution is performed for the non-homogeneous Fourier transformed equation. We mention that the model was adapted as much as possible to cope with the experimental set-up and conditions specified in the next section and shown in figure 2(a). For example the focusing conditions were taken into account and the radial beam profile was considered as Gaussian for the input beam in the fiber. Also, for the gas density along the microchannel axis we used the values plotted in figure 1(c).

Figures 4(a) and (b) show the calculated harmonic field of a selected number of harmonics as a function of the waveguide axial coordinate (z) for two different gas backing pressures. The numerical gas density distributions along the waveguide obtained from COMSOL analysis are reported as dotted lines. The selected harmonic orders range from the 55-th (85 eV, 14.4 nm) to the 119-th (185.5 eV, 6.7 nm).

It can be noticed that the harmonic field coherently builds up through the channel to a point of maximum amplitude which depends on both the harmonic order and the gas density. In fact, the build-up of harmonics along the hollow waveguide is strongly affected by phase-matching and absorption that can hinder the cumulative growth of the harmonic field during the propagation in the waveguide and are responsible for the appearance of peaks in the amplitude. These peaks are spatially dispersed since both phase matching and absorption are wavelength sensitive. For the cases reported in figure 4, lower harmonic orders reach a maximum for a longer propagation distance due to a longer coherence length.

By inspection of figures 4(a) and (b), it can be noticed that the source for the harmonics is proportional to the gas density profile that contributes to shaping the build-up of the total field which, on the other hand, is affected by the suppression mechanisms. More specifically, by increasing the pressure as in 4(b), the coherence length changes and leads to a shift of the peaks towards shorter z values. In this case, a considerable depletion along the hollow waveguide occurs, which is more pronounced for the lower orders. Despite the detrimental effect produced by decoherence, higher densities as in 4(b) are beneficial to the

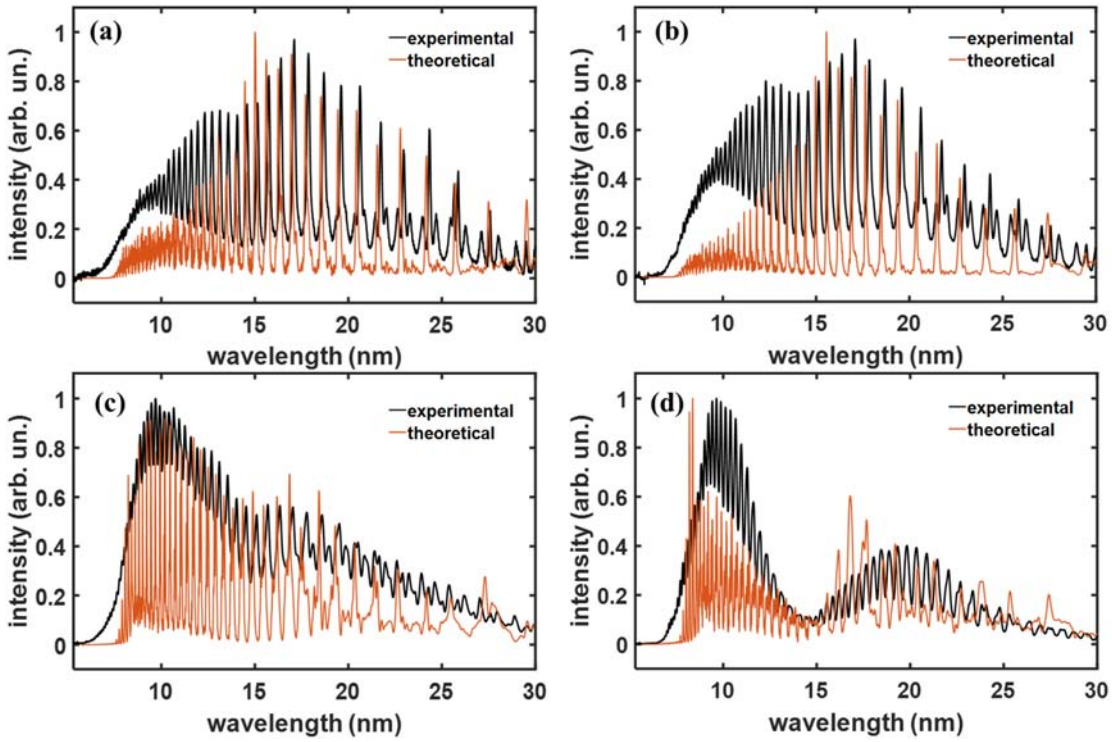

Figure 5. Comparison between experimental HHG spectra for different gas densities inside the device. The black curves represent the experimental spectra acquired for (a) 50 mbar, (b) 100 mbar, (c) 200 mbar and (d) 600 mbar. The corresponding theoretical spectra are calculated by using numerical gas densities obtained for a reservoir pressures of (a) 100 mbar, (b) 200 mbar, (c) 600 mbar and (d) 1 bar.

generation yield, which is two order of magnitude higher than in 4(a). By accounting for this pressure dependence and by accurately studying the structure of the micro-fluidic device, it will be possible to achieve a further improvement in the harmonic generation yield, thus reducing destructive effects of decoherence for longer propagation distance. However, due to the peak dispersion as a function of the harmonic order, yield optimization can be achieved only within a limited portion of the spectrum.

The comparison between experimental and theoretical HHG spectra for different gas densities is provided in figure 5. Here, the spectral dependence on the gas density observed experimentally is reproduced by the theoretical spectra. Indeed, the spectra obtained by calculations show a reshaping upon increasing gas pressures, corresponding to the increase of harmonic yield at higher photon energies as well as a strong suppression of the lower harmonics that is consistent with the experimental observations. As already mentioned, the experimental spectra are affected by the second-order diffraction of the spectrometer, which produces a replica of the HHG spectrum at longer wavelength. The second order-induced artifact is partially overlapped with the HHG signal and is responsible for the appearance of side peaks, which are not taken into account in the theoretical calculations. The theoretical calculations are in very good qualitative agreement with the experimental results. However, the theoretical spectra are calculated assuming a backing pressure in the reservoir higher than the experimental one. This discrepancy can be due to several effects. The numerical calculations do not take into account plasma effects at the entrance of the hollow waveguide and the estimation of the ionization rate by ADK [22] may be different from the experimental one. Furthermore, the numerical method used for computing the gas density profiles along the waveguide does not include rarefaction effects which may play a non-negligible role at our pressure range.

If compared to the typical high-harmonics generation geometry based on gas-jets, capillaries offer the advantage that XUV emission arises from an extended medium with controllable gas density [21, 23]. Indeed, the waveguide-assisted confinement of the laser beam allows to extend the interaction region through the whole waveguide, thus involving a number of emitters larger than in a tight-focusing geometry. However, for generating bright HHG spectra, the emission produced by all the emitters along the channel must add in phase.

In this sense, capillaries are particularly suitable for phase-matching optimization, since they enable to balance the anomalous dispersion of the neutral gas with the normal dispersion of the waveguide and the free electrons [29]. On the other hand, when an intense pulse is focused into a gas jet, phase matching is prevented by the relative phase shifts of the fields as they come across the focus (the so-called Gouy phase

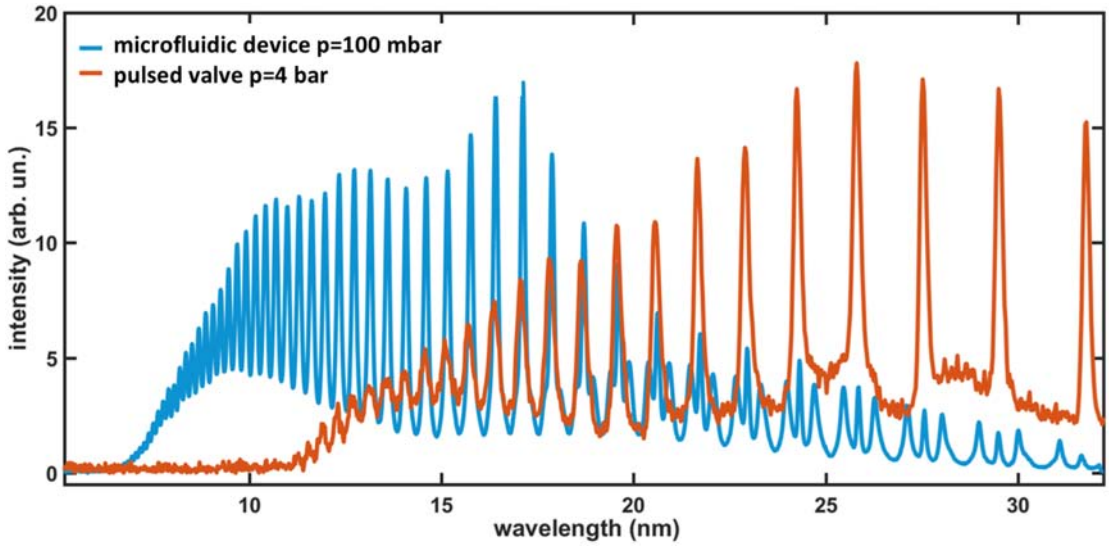

Figure 6. Comparison between HHG spectra produced in helium inside the microfluidic device (blue) and in a pulsed gas jet (red). The pulse gas jet spectra intensity is multiplied by 10.

shift). Even if this effect can be partially overcome by displacing the gas-jet after the focus, the extension of the interaction region remains strongly limited because of the divergence of the beam.

We compared the HHG yield inside the gas-filled microchannel with that achieved in the most commonly used interaction geometry involving a gas-jet. Figure 6 shows a harmonics spectrum generated in the channel with a 100 mbar backing pressure of helium (blue line) and an HHG spectrum generated in a helium pulsed-jet at a 4-bar backing pressure (red line, x10 magnification). The pulsed jet is produced by a solenoid pulse valve with a 500 μm nozzle working at a 20 Hz repetition rate. In this regime, a high backing pressure (4 bar) was used to reproduce the standard working conditions of our HHG beamlines and the related harmonics spectrum was acquired in optimized conditions. Both the two spectra were rescaled in order to compare single-shot operation. An extended cutoff, up to 6.5 nm (190 eV), is obtained inside the microchannel, whereas a cutoff of about 11 nm (110 eV) is observed in the jet. Moreover, an estimation of the harmonic generation yield in the spectral region detected by the spectrometer can be performed by integration of the HHG spectra. As a result, a higher generation yield is achieved in the microchannel, where the overall spectral intensity is over 20 times the one obtained with the pulsed jet. For improving HHG in pulsed jets, higher gas pressures and pulsed valves with a higher repetition rates can be exploited, but more sophisticated and properly designed pumping systems are required. In this framework, the micro-chip has the advantage that provides better performances with lower gas densities, thus requiring a less demanding vacuum technology.

As already discussed, by increasing the pressure above 100 mbar an even brighter and broader spectral cutoff can be obtained in the microchannel. However, at higher pressures, the effects of phase-matching and absorption become dominant leading to a selective suppression of the low-order harmonics.

Although we achieved an overall improvement of the generation yield in comparison to traditional HHG by gas-jets, we foresee that a further improvement in the harmonic generation can be obtained by overcoming the phase-matching limitations. Practical approaches exploiting Quasi Phase Matching (QPM) have already been demonstrated. In particular, two main strategies are known to be effective in improving the HHG yield: the modulation of the driving field intensity and the modulation of the gas density. As proved by Gibson *et al* a considerable improvement in the conversion efficiency and spectral extension of HHG can be obtained through modulation of the driving field intensity produced by a modulation of the hollow-waveguide diameter [23]. Moreover, Seres *et al* reported on the coherent build-up of soft-x-rays in a gas medium with a modulated density obtained by juxtaposition of two gas sources [30]. This approach demonstrates the possibility to optimize the photon flux of a pattern of HHG-based sources by appropriate positioning of them in a focused laser beam and it is scalable to a higher number of sources [31].

We can exploit the strong capabilities of FLICE technique to prototype microfluidic architectures that could allow the implementation on-chip of all these methods, either separated or together. By doing this, we expect to boost the generation yield by more than one order of magnitude with respect to the already good performance of the first-generation devices. Moreover, FLICE allows to realize microfluidic devices with

arbitrarily complex and non-axisymmetric internal structure which outperforms that provided by standard glass machining technique of hollow-core fiber for ultrafast applications.

5. Conclusions

We have demonstrated efficient generation of high-order harmonics in helium through a microfluidic device realized by femtosecond-laser-micromachining followed by chemical etching. The performances of these devices surpass that produced by standard pulsed gas-jets in terms of both efficiency and spectral extension. We performed theoretical calculations taking into account the propagation of the driving field in the device, showing a good agreement with the experimental results. By exploiting the extreme flexibility of the FLICE technique, more complex microfluidic devices can be realized, aiming at further improving the HHG efficiency in a Quasi Phase-Matching regime.

Furthermore, using longer wavelength driving pulses and optimizing phase-matching conditions, we expect to achieve efficient harmonic generation in the soft-X region approaching the water window, thus providing an ideal source for attosecond time resolved spectroscopy in the XUV and x-ray energy regime.

Moreover, by integrating several functionalities (attosecond pulse generation, spectral acquisition etc.) inside the same device, on-chip platforms for HHG and attosecond spectroscopy, in both liquid and gas phases, can be realized. This achievements will mark a substantial breakthrough in ultrafast technology, potentially making HHG-based sources available for application in numerous novel fields.

Acknowledgment

This study was supported by the European Union's Horizon 2020 research and innovation program under the Marie Skłodowska-Curie projects ASPIRE (Grant No. 674960), by the European Research Council Proof of Concept Grant FESTA (Grant No. 813103), by the Italian Ministry of Research and Education with the projects ELI–ESFRI Roadmap and PRIN aSTAR, by the Consiglio Nazionale delle Ricerche with the Joint Laboratory ATTOBIO. V. Tosa acknowledges mobility support from Project no. 32PFE/18 of Romanian UEFISCDI.

ORCID iDs

A G Ciriolo https://orcid.org/0000-0003-1189-329X
R Martínez Vázquez https://orcid.org/0000-0001-8728-5819
V Tosa https://orcid.org/0000-0002-2716-6874
A Frezzotti https://orcid.org/0000-0003-3858-1536
G Crippa https://orcid.org/0000-0002-0157-4968
M Devetta https://orcid.org/0000-0002-3806-3475
D Faccialá https://orcid.org/0000-0002-5072-0394
F Frassetto https://orcid.org/0000-0001-5528-1995
L Poletto https://orcid.org/0000-0002-0914-0531
A Pusala https://orcid.org/0000-0003-1825-508X
C Vozzi https://orcid.org/0000-0002-0212-0191
R Osellame https://orcid.org/0000-0002-4457-9902
S Stagira https://orcid.org/0000-0002-8457-3185

References

[1] Lewenstein M *et al* 1994 Theory of high-harmonic generation by low-frequency laser fields *Phys. Rev.* A **49** 2117
[2] Scrinzi A *et al* 2005 Attosecond Physics *J. Phys. B: At. Mol. Opt. Phys.* **39** R1
[3] Krausz F and Ivanov M 2009 Attosecond Physics *Rev. Mod. Phys.* **81** 163
[4] McPherson A *et al* 1987 Studies of multiphoton production of vacuum-ultraviolet radiation in the rare gases *JOSA* B **4** 595
[5] Ferray M *et al* 1988 Multiple-harmonic conversion of 1064 nm radiation in rare gases *J. Phys. B: At. Mol. Opt. Phys.* **21** L31
[6] Calegari F *et al* 2016 Advances in attosecond science *J. Phys. B: At. Mol. Opt. Phys.* **49** 062001
[7] Kühn S *et al* 2017 The ELI-ALPS facility: the next generation of attosecond sources *J. Phys. B: At. Mol. Opt. Phys.* **50** 132002
[8] Davis K M *et al* 1996 Writing waveguides in glass with a femtosecond laser *Opt. Lett.* **21** 1729
[9] Gattass R R and Mazur E 2008 Femtosecond laser micromachining in transparent materials *Nat. Photon.* **2** 219
[10] Osellame R, Cerullo G and Ramponi R 2012 *Femtosecond Laser Micromachining: Photonic and Microfluidic Devices in Transparent Materials* (Berlin: Springer) vol **123**
[11] Hnatovsky C *et al* 2006 Fabrication of microchannels in glass using focused femtosecond laser radiation and selective chemical etching *Appl. Phys.* A **84.1–2** 47
[12] Osellame R *et al* 2011 Femtosecond laser microstructuring: an enabling tool for optofluidic lab-on-chips *Laser and Photonics Rev.* **5** 442

[13] Sima F et al 2018 Three-dimensional femtosecond laser processing for lab-on-a-chip applications *Nanophotonics* **7** 613
[14] Galli M et al 2019 Generation of deep ultraviolet sub-2-fs pulses *Opt. Lett.* **44** 1308
[15] Nisoli M et al 1998 Toward a terawatt-scale sub-10-fs laser technology *IEEE J. Sel. Top. Quantum Electron.* **4** 414
[16] Travers J C et al 2011 Ultrafast nonlinear optics in gas-filled hollow-core photonic crystal fibers *J. Opt. Soc. Am.* B **28** A11
[17] Durfee C G et al 1999 Intense 8-fs pulse generation in the deep ultraviolet *Opt. Lett.* **24** 697
[18] Misoguti L et al 2001 Generation of broadband VUV light using third-order cascaded processes *Phys. Rev. Lett.* **87** 013601
[19] Russell P S et al 2014 Hollow core photonic crystal fibres for gas-based nonlinear optics *Nat. Photon.* **8** 278
[20] Ciriolo A G et al 2018 Generation of ultrashort pulses by four wave mixing in a gas-filled hollow core fiber *J. Opt.* **20** 125503
[21] Popmintchev T et al 2012 Bright coherent ultrahigh harmonics in the keV x-ray regime from mid-infrared femtosecond lasers *Science* **336** 1287
[22] Ammosov M V et al 1986 Tunnel ionization of complex atoms and of atomic ions in an alternating electric field *Sov. Phys. JETP* **64** 1191
[23] Gibson E A et al 2003 Coherent soft x-ray generation in the water window with quasi-phase matching *Science* **302** 95
[24] COMSOL Multiphysics® v. 5.4. (Stockholm: COMSOL AB) (www.comsol.com)
[25] Tosa V et al 2003 Generation of high-order harmonics in a self-guided beam *Phys. Rev.* A **67** 063817
[26] Tosa V et al 2005 High-order harmonic generation by chirped and self-guided femtosecond laser pulses. I. Spatial and spectral analysis *Phys. Rev.* A **71** 063807
[27] Tosa V et al 2005 High-order harmonic generation by chirped and self-guided femtosecond laser pulses. II. Time-frequency analysis *Phys. Rev.* A **71** 063808
[28] Nurhuda M et al 2003 Propagation dynamics of femtosecond laser pulses in hollow fiber filled with argon: constant gas pressure versus differential gas pressure *J. Opt. Soc. Am.* B **20** 2002
[29] Durfee C G et al 1999 Phase matching of high-order harmonics in hollow waveguides *Phys. Rev. Lett.* **83** 2187
[30] Seres J et al 2007 Coherent superposition of laser-driven soft-x-ray harmonics from successive sources *Nat. Phys.* **3** 878
[31] Pirri A et al 2008 Enhancing the yield of high-order harmonics with an array of gas jets *Phys. Rev.* A **78** 011801